Fire Safety Journal 140 (2023) 103835

Contents lists available at ScienceDirect

Fire Safety Journal

journal homepage: www.elsevier.com/locate/firesaf

Experimental study of fire containment using water mist curtains in a reduced-scale deck of a ro-ro ship

Davood Zeinali [a,1,*], Rabah Mehaddi [a], Florian Ingold [a], Gilles Parent [a], Zoubir Acem [a], Anthony Collin [a], Jose Luis Torero [b], Pascal Boulet [a]

[a] Université de Lorraine, CNRS, LEMTA, F-54000, Nancy, France
[b] Department of Civil, Environmental & Geomatic Engineering, University College London, London, UK

ARTICLE INFO

Keywords:
Water mist curtain
Containment
Smoke
Ro-ro ship
Open deck
Closed deck

ABSTRACT

Experiments have been conducted to evaluate the containment of smoke and heat using water mist curtains in a model setup of a ro-ro ship's cargo deck with a scale of 1:13, providing practical insights into the application of such fire protection systems in the cargo deck as well as valuable data for future numerical simulations. In this regard, the requirements of the international convention of Safety of Life at Sea (SOLAS) are studied for the side openings of so-called 'open decks' in comparison with 'closed decks', especially to examine the feasibility of using water mist curtains for creating isolated subdivisions in the ro-ro space as a fire management strategy. The water mist curtains are created with one or two rows of water mist nozzles at pressures ranging from 3 to 8 bar, while the source of smoke and heat is a liquid pool fire, and inert cargo items are used in some experiments. Correspondingly, the interaction between the water mist curtain(s) and the fire is evaluated in terms of its heat release rate, and the containment effect is quantified via measurements of smoke flow through the deck and through the windows, concentrations of gaseous species, as well as gas temperatures at various key locations. The study shows that water mist curtains have a strong effect on fire dynamics and smoke propagation, but containment is dependent on the configuration of side openings and the location of fire, among other important factors.

1. Introduction

Roll-on/roll-off vessels, commonly referred to as ro-ro ships, are large ships used to transport wheeled cargo such as trucks and trailers, loaded onto the ship using built-in ramps. Ro-ro ships can also be passenger ships, customarily known as ferries. Ro-ro ships are characterized by very large uncompartmentalized spaces that can allow the development of extensive fires with potentially devastating consequences. Accordingly, to reduce the cost and potential consequences of fires aboard such ships, it is necessary to study means to contain heat and smoke in their long cargo decks. Compartmentation of such spaces by means of active fire protection systems has received little attention and remains a significant challenge for computational models, and thus the spread of smoke, heat and fire still needs to be characterized by means of experiments. Correspondingly, experiments have been conducted in this study in a model setup of a ro-ro ship's cargo deck to evaluate the possibility of containment by means of active fire protection systems, namely, using water mist curtains. Mist in this context refers to a fine water spray in which 99% of the spray volume consists of droplets with diameters less than 1000 μm [1].

Fire containment by water mist curtains has been widely explored in the literature in various contexts [2–6]. In the context of ro-ro ships, thermal radiation containment using water mist curtains was investigated by Zeinali et al. [7] who used an electric black body at a fixed temperature of 550 °C and quantified the radiation levels with and without water mist curtains using a multispectral infrared camera. Conversely, smoke containment using water mist curtains and under levels of confinement common in the maritime context is understudied. Note that the space of a ship is divided into several levels called decks. When compared to the geometry of a building or a tunnel, the dimensions of a typical cargo deck on a ro-ro ship are quite unique. The decks typically have a length that is between 4 and 6 times its width. In the event of a fire in such a geometry, there will be a transient period where the smoke will propagate in all directions of the space. This period

* Corresponding author. Tillerbruvegen 202, 7092, Tiller, Norway.
E-mail address: davood.zeinali@risefr.no (D. Zeinali).
[1] Current affiliation: RISE Fire Research, Trondheim, Norway.

https://doi.org/10.1016/j.firesaf.2023.103835
Received 16 September 2022; Received in revised form 6 April 2023; Accepted 28 May 2023
Available online 7 June 2023

will be followed by a second stage where the flow is unidimensional, i.e., the flow will be largely in the longer direction of the deck. The present experimental study considers the impact of the ship's cargo deck geometry on the water mist curtain and its capability for containment of smoke and heat to mitigate fire hazards. In particular, the requirements of the International Convention for the Safety of Life at Sea (SOLAS) are studied for the side openings of so-called 'open ro-ro decks' in comparison with 'closed ro-ro decks'. Based on SOLAS chapter II-2, Part A, Regulation 3 [8], an 'open deck' has permanent openings distributed in the side plating or deckhead or from above, having a total area of at least 10% of the total area of the space sides, e.g., as shown in Fig. 3. Smaller openings constitute a 'closed deck'. This is regardless of the deck being open at one or both ends, or neither end. The present study assesses the influence of these definitions on fire dynamics in the deck, especially to examine the feasibility of using water mist curtains in the ro-ro space as a fire management strategy.

The experiments are conducted in a reduced-scale setup (Fig. 1), consisting of a model cargo deck with a scale of approximately 1:13 with respect to the inner dimensions of the closed deck of a typical ro-ro ferry, i.e., Stena Jutlandica shown in Fig. 2. The choice of the scaling ratio was very prohibitive and was limited to 1:13 due to the extensive length required for the model setup, i.e., 8 m. The deck height is the smallest dimension of ro-ro ship decks, making it the primary limiting geometrical factor in the problem which is modeled precisely to 1:13 scale. The width and length of the model deck are scaled approximately after some manufacturing considerations.

The objective of the experiments is to study the effects on containment from several key parameters: a) the fire location, b) the fire size, c) the source fuel, d) the windows, e) the two ends of the deck, f) cargo presence or absence, g) the number of water mist curtains, h) the distance and configuration of curtains, as well as i) the water pressure at the nozzles. An aluminum lid is used to close the side of the deck near the fire in most experiments, but the lid is not shown in Fig. 1 to visualize the interior.

2. Methodology

For reasons of safety and repeatability, the fire is created using 135–140 g heptane or diesel (comparable to fossil fuels in conventional vehicles) in a circular pan that has a depth of 0.04 m and an inner diameter of 0.13 m or 0.15 m. Fig. 1 shows a schematic of the model cargo deck setup. The model is a corridorlike compartment and has a scale of 1:13 with respect to the inner dimensions of the closed deck of Stena Jutlandica shown in Fig. 2 (refer to section 1 for explanations regarding the choice of scaling). The setup is split into 4 detachable sections, each measuring 2 m in length, which can be moved to rearrange the deck as desired for different tests.

As shown in Fig. 1, the spray system was designed by the authors to contain two rows of water mist curtains, allowing to split the deck into a maximum of three isolated subdivisions upon the activation of both curtains at the same time. Each curtain is made with 19 water mist nozzles (type TP400067 from Spraying Systems Co. with an orifice diameter of 530 μm). Between each two successive nozzles, there is 0.1 m distance, and the nozzles are at 0.38 m height with respect to the floor of the deck in the setup, i.e., the injection point of the nozzles is at 0.02 m from the deck's ceiling.

The spray pattern of the used water mist nozzles resembles an elliptical cone which can be characterized using one large angle (a_1) and one small angle (a_2) as shown in Fig. 4. The nozzles are fixed such that the large spray angle aligns with the width of the deck (measuring 2 m as shown in Fig. 1) while the small spray angle is aligned with the length of the deck. Correspondingly, the consecutive nozzles have overlapping spray patterns dominantly along the length of the water mist curtain (see Fig. 4), consolidating the curtain as a vertical barrier for radiation and smoke. Although this elliptical spray pattern is rather common, other nozzles with different spray patterns are available in the market, but an analysis of the full range of available spray patterns was beyond the scope of this study. The spray angles a_1 and a_2 for the used nozzles are presented in Table 1 for the water pressures tested in the present study.

The feed water system features a compressor capable of providing air with a maximum pressure of 10 bar (Fig. 4). Using a pressure regulator, the air is stored at the desired pressure in an air tank. This regulated

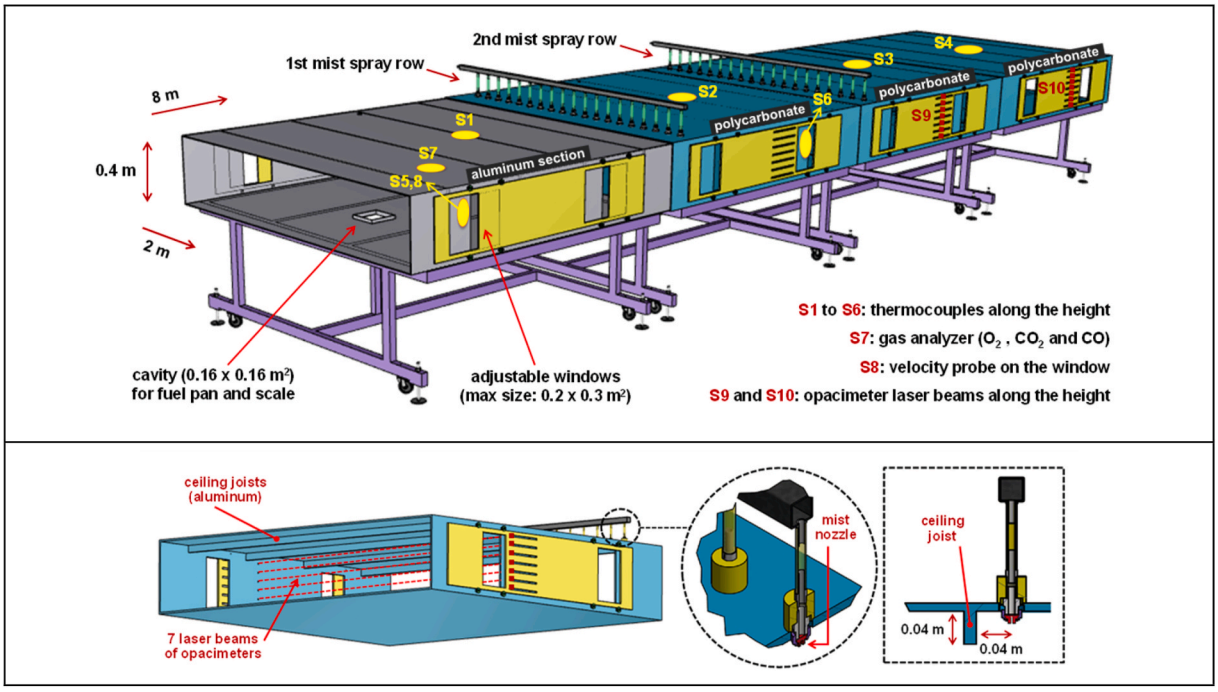

Fig. 1. Set-up of the reduced-scale experiments (top), consisting of one aluminum section for the fire zone, and three transparent polycarbonate sections (bottom), each 2 m long.

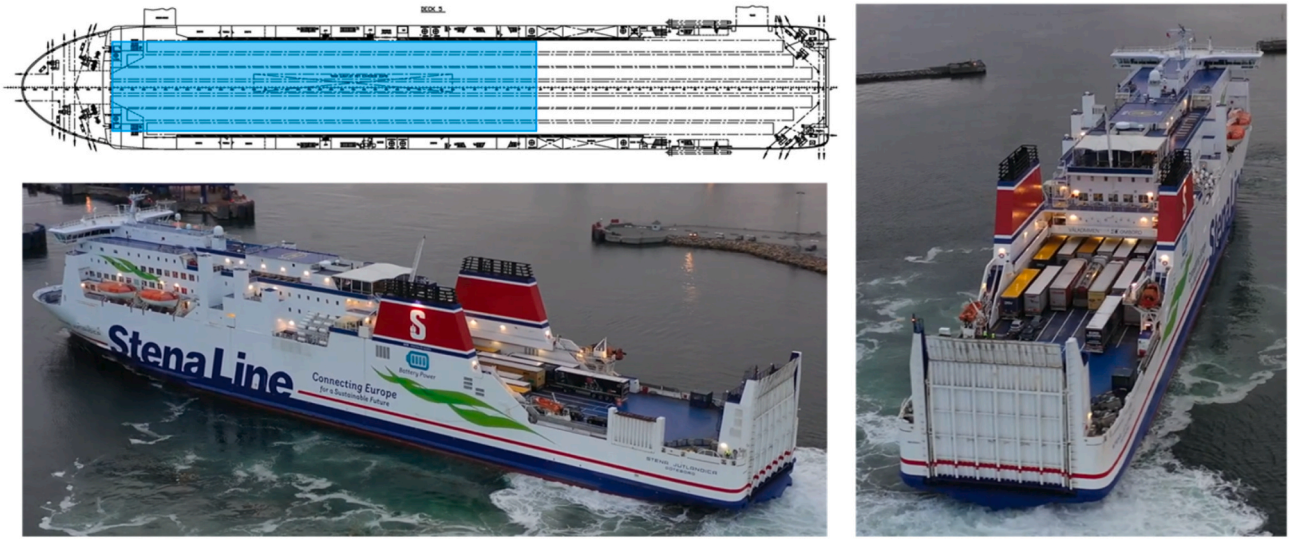

Fig. 2. A typical ro-ro ferry (Stena Jutlandica) and its 'closed deck' containing trailers.

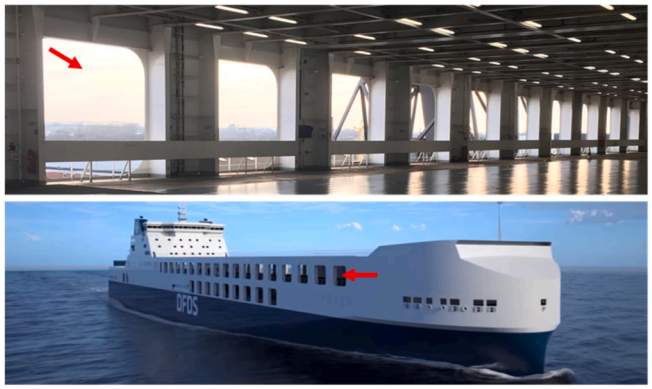

Fig. 3. Typical side openings of an open deck on a ro-ro ship (Hollandia Seaways).

supply of air is then used to pressurize the feedwater in the water tank, capable of holding up to 30 L of water. Correspondingly, the feedwater tank provides pressurized water to the two rows of water mist nozzles, with a pressure gauge at the center of each row recording the pressure with an accuracy of 10 millibar. Moreover, two flowmeters are used to monitor the total flowrate of each spray row with an accuracy of 0.1 L/min, and several valves are used to allow the regulation of pressure and water supply as desired. This feed water setup is similar to that used by Parent et al. [5].

Even though the geometrical size of the model is 1/13th of the considered real-scale deck (see explanations in section 1), a different scaling factor is needed for the design of the flow rate and droplet diameter of the water mist curtains in the reduced-scale model. While a general scaling approach is presented by Quintiere [9] and a useful summary of the related heat transfer relations has been provided by Drysdale [10], for the specific application of fire suppression systems, the most relevant scaling relations have been reported by Yu [11]. The SFPE Handbook of Fire Protection Engineering [12] provides a summary of the related characteristics of water mist systems. Table 2 shows the scaling of the model setup's different features with respect to those of a ro-ro ship based on the aforementioned principles.

A wide range of fire scenarios have been considered in the experiments (see Tables 3 and 4). This includes different locations for the fire source section (i.e., section 1 shown in Figs. 6–8), such that the fire

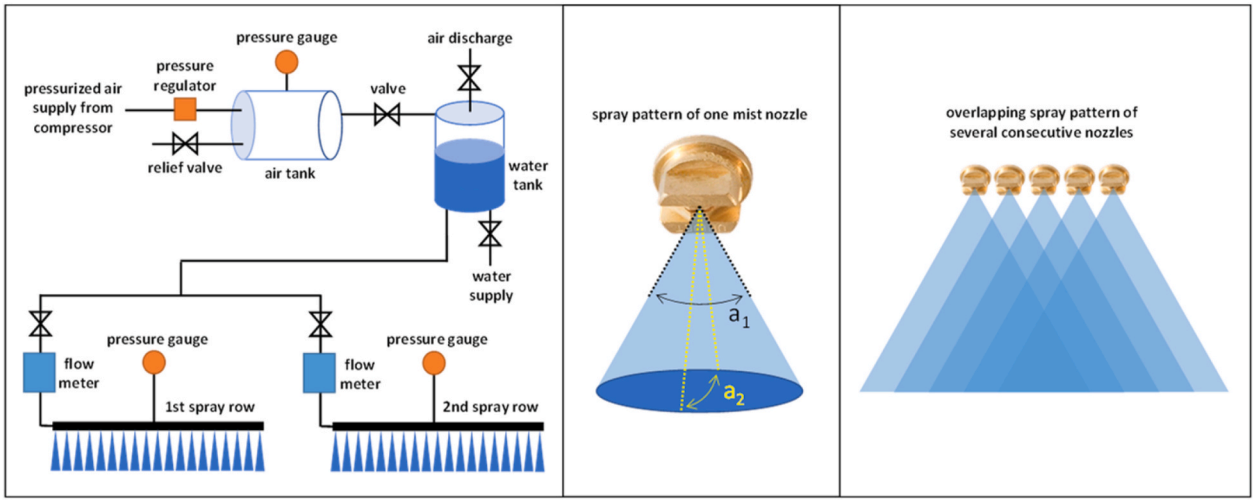

Fig. 4. Setup of feed water system for the two water mist curtains (left), the spray pattern of a single water mist nozzle (middle), and spray pattern of several consecutive nozzles (right).

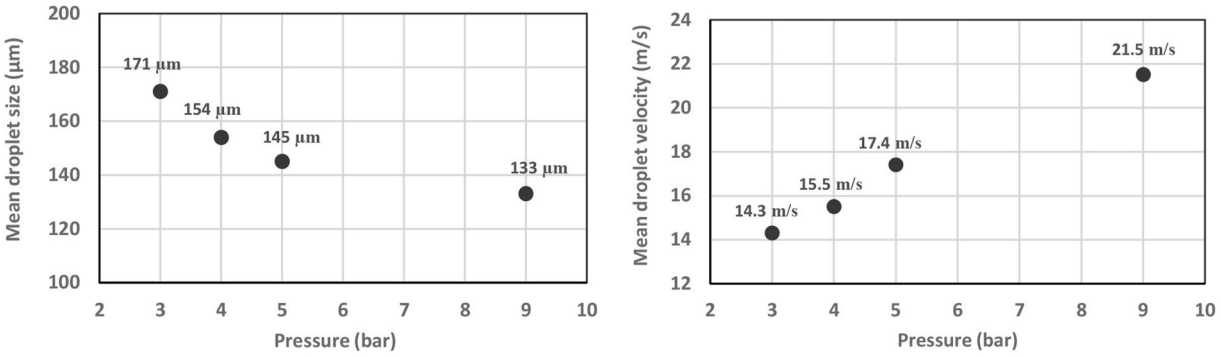

Fig. 5. Mean droplet diameter, i.e., D50 in μm (left) and mean droplet velocity, i.e., V50 in m/s (right) measured at 0.2 m distance below the injection point of one water mist nozzle.

Table 1
The flow rate and spray angles of the water mist nozzles in the present study.

Pressure[a] [bar]	3	5	8
Flow rate[a] [L/min]	0.2	0.3	0.4
Large angle of spray[b] [°]	40	50	55
Small angle of spray[b] [°]	17	19	21

[a] Water pumps on ro-ro ships can typically provide 1800–16,000 L/min water at pressures between 3 and 8 bar.
[b] Angles shown in Fig. 4.

Table 2
The scale of the model setup with respect to the closed deck of Stena Jutlandica shown in Fig. 2

Feature	Model setup	Ship	Scaling factor
Deck height [m]	0.4	5.2	$\alpha = 13$
Deck length [m]	8	97	$\alpha \approx 13$
Deck width [m]	2	23	$\alpha \approx 13$
Water flow rate per nozzle [L/min]	0.2–0.4	122-244[a]	$\alpha^{5/2}$ [b] $= 609$
Mean diameter of droplets [μm]	130-170[c]	460–600	$\alpha^{1/2}$ [b] $= 3.6$
Mean velocity of droplets [m/s]	14-22[c]	50–79	$\alpha^{1/2}$ [b] $= 3.6$

[a] The water pumps on ro-ro ships can typically provide 1800–16,000 L/min at pressures between 3 and 8 bar.
[b] Based on scaling correlations reported by Yu [11].
[c] Droplet velocities (shown in Fig. 5) are expected to be in the order of gas velocities at that location in the setup.

Table 3
Target study parameters (see Table 4 for the conducted fire experiments).

Parameter	Option 1	Option 2	Option 3
Fire location[a]	End of deck (Figs. 6 and 7)	Middle of deck (Fig. 8)	–
Deck ends	Closed only on the fire side	Closed on both ends	Open on both ends
Fire size[b]	0.15 m diameter heptane pool	0.15 m diameter diesel pool	0.13 m diameter diesel pool
Fuel	Heptane (0.15 m diameter pool)	Diesel (0.13–0.15 m diameter pool)	–
Area of windows[c]	15% of sides (open deck)	0% of sides (closed deck)	–
Cargo load in deck	None	Full (inert boxes ≈ vehicles)	–
Curtain row	First	Second	Both
Distance of curtains	2 m	2.4 m	0.4 m
Curtain configuration	Series	Straddle	–
Flow rate per nozzle	0.4 L/min (8 bar)	0.3 L/min (5 bar)	0.2 L/min (3 bar)

[a] For the precise definition of the fire scenarios, refer to the captions of Table 4.
[b] To put the real-scale fire sizes in perspective, option 1 is roughly comparable to a 17 MW truck fire and option 3 to a 4 MW car fire.
[c] 'Windows' here refer to permanent openings distributed in the side plating as shown in Fig. 3.

source is either at one end of the deck or at the center, while the deck is left open on both ends or it is sealed on one or both ends using an aluminum wall (see also caption of Table 4 for the fire scenario abbreviations). Moreover, the scenarios include different configurations for the fire size, fuel type, area of the windows, cargo load in the deck, number of curtains, water flow rate, as well as distance and configuration of curtains.

In each experiment, the fire is allowed to burn freely for 3 min, after which the curtains are activated and remain operational for 2 min. The containment effects are then evaluated through the measurements of gas temperatures at various locations along the height of the deck and on the windows, but also through the measurements of gas velocities from the window opposite the fire. In addition, the mass of the pool is recorded with a scale to estimate the Heat Release Rate (HRR) of the fire using the effective heat of combustion of the fuel (see explanations for Fig. 16 regarding the HRR estimations). Furthermore, the efficiency of combustion is monitored by measuring the concentrations of gaseous species near the fire either using a gas analyzer of model Testo350 or using a gas analyzer of model Testo350 M/XL (see Figs. 6–8 for the location of the measurement sensors). Moreover, opacity measurements are made as shown in Fig. 1 along the height of the deck using 14 laser beams with a wavelength of 640 nm modulated at a frequency of 360 Hz, spanning the 2 m width of the deck before being detected and demodulated. The modulation of the beams eliminates the effects from the ambient light and provides a stable signal, making it possible to detect transmissions as low as 10^{-5}, with 'transmission' being the ratio of light intensity with smoke to light intensity without smoke [13].

The interactions of fire with the space and the water mist are interdependent and scaling will influence these interactions. To examine the impact of HRR on containment as a separate study parameter, the present study considers three different fire sources, namely, 0.13 m and 0.15 m diesel pools and 0.15 heptane pools, with HRR profiles ranging from 3 to 20 kW in the absence of water mist curtains.

3. Phenomenological observations

After the fuel is ignited, the resulting fire starts to generate radiative and convective heat as well as combustion products in the form of smoke. Given that smoke is hotter than the ambient air, it rises due to buoyancy and accumulates below the ceiling, resulting in an upper layer of smoke and a lower layer of ambient air. Although open windows allow part of the generated smoke to exit the deck, a significant portion of the smoke is observed to spread through the deck longitudinally if no barrier is present. Placing water mist curtains along the length of the

Table 4
Experiments conducted in the reduced-scale deck setup shown in Fig. 1. Highlights indicate changes made with respect to the first test.

Test ID#	Fuel	Fire size	Fire scenario	Area of openings	Water mist curtain(s)[a]	Flow rate per nozzle	Distance of curtains	Curtain configuration	Cargo load
2	Diesel	Ø 0.13 m pan	E1[b]	15%	first and second water mist curtains	0.3 L/min	2 m	Series	None
8	Diesel	Ø 0.15 m pan	E1[b]	15%	first and second water mist curtains	0.3 L/min	2 m	Series	None
9	Diesel	Ø 0.15 m pan	E1[b]	15%	No curtain	--	--	--	None
11-2	Heptane	Ø 0.15 m pan	E1[b]	15%	No curtain	--	--	--	None
14	Heptane	Ø 0.15 m pan	E1[b]	15%	second water mist curtain	0.4 L/min	--	--	None
15	Heptane	Ø 0.15 m pan	E1[b]	15%	first water mist curtain	0.4 L/min	--	--	None
17	Heptane	Ø 0.15 m pan	E1[b]	15%	first and second water mist curtains	0.3 L/min	2 m	Series	None
19	Heptane	Ø 0.15 m pan	E1[b]	15%	first water mist curtain	0.2 L/min	--	--	None
25	Heptane	Ø 0.15 m pan	E1[b]	0%	first and second water mist curtains	0.3 L/min	2 m	Series	None
28	Heptane	Ø 0.15 m pan	E1[b]	0%	second water mist curtain	0.4 L/min	--	--	None
30	Heptane	Ø 0.15 m pan	E1[b]	0%	first and second water mist curtains	0.4 L/min	2 m	Series	None
41	Heptane	Ø 0.15 m pan	E1[b]	0%	first and second water mist curtains	0.4 L/min	0.4 m	Series	None
42	Heptane	Ø 0.15 m pan	E1[b]	0%	first and second water mist curtains	0.3 L/min	0.4 m	Series	None
43	Heptane	Ø 0.15 m pan	E1[b]	0%	first and second water mist curtains	0.2 L/min	0.4 m	Series	None
47	Heptane	Ø 0.15 m pan	M1[b]	15%	No curtain	--	--	--	None
51	Heptane	Ø 0.15 m pan	M1[b]	15%	first and second water mist curtains	0.2 L/min	2.4 m	Straddle[c]	None
73-3	Heptane	Ø 0.15 m pan	E1[b]	15%	No curtain	--	--	--	Full[d]
73-4	Heptane	Ø 0.15 m pan	E1[b]	15%	No curtain	--	--	--	Full[d]
74	Heptane	Ø 0.15 m pan	E1[b]	0%	No curtain	--	--	--	Full[d]
77	Heptane	Ø 0.15 m pan	E1[b]	15%	first water mist curtain	0.3 L/min	--	--	Full[d]
78	Heptane	Ø 0.15 m pan	E1[b]	0%	first water mist curtain	0.3 L/min	--	--	Full[d]
80	Heptane	Ø 0.15 m pan	E1[b]	0%	first water mist curtain	0.4 L/min	--	--	Full[d]
81	Heptane	Ø 0.15 m pan	E1[b]	15%	first water mist curtain	0.4 L/min	--	--	Full[d]
82	Heptane	Ø 0.15 m pan	E1[b]	15%	first water mist curtain	0.2 L/min	--	--	Full[d]
83	Heptane	Ø 0.15 m pan	E1[b]	0%	first water mist curtain	0.2 L/min	--	--	Full[d]
86	Heptane	Ø 0.15 m pan	E1[b]	15%	first and second water mist curtains	0.4 L/min	2 m	Series	Full[d]
88	Heptane	Ø 0.15 m pan	E0[b]	15%	No curtain	--	--	--	Full[d]
96	Heptane	Ø 0.15 m pan	E2[b]	15%	No curtain	--	--	--	Full[d]
101	Heptane	Ø 0.15 m pan	E2[b]	15%	first and second water mist curtains	0.4 L/min	2 m	Series	Full[d]

a The first and second curtain rows are fixed at the locations shown in **Error! Reference source not found.**.

b The fire scenario abbreviations indicate, firstly, the location of the fire: 'E' = end of deck (Figs. 1 and 2), and 'M' = middle of deck (Fig. 3); and secondly, the presence of walls that close the deck from either end: '0' = no walls on either end of the deck, '1' = one wall closing the deck on the fire side, '2' = two walls closing the deck from both ends.

c In the 'straddle' configuration, the fire section is the second section along the deck, such that two water mist curtains can straddle the fire and contain it from both sides with a distance of 2.4 m from one another.

deck reduces this longitudinal spread of smoke and helps contain the heat near the fire. In addition, the smoke stratification is broken, i.e., the upper smoke layer is mixed with the lower ambient layer, although the amount of smoke decreases with distance from the fire as illustrated in Figs. 9 and 10. The mixed environment that contains smoke and water mist is expected to hinder the development of fire because of the reduced clean air and the enhanced cooling near the fire source. Furthermore, when the fire is close to the water mist curtain, the flames are fanned if the water pressure is high.

In the present work, we quantify the reduction of longitudinal smoke flow offered by water mist curtains, explicitly by analyzing the volume fraction of soot, i.e., particulate smoke consisting of carbonaceous par-

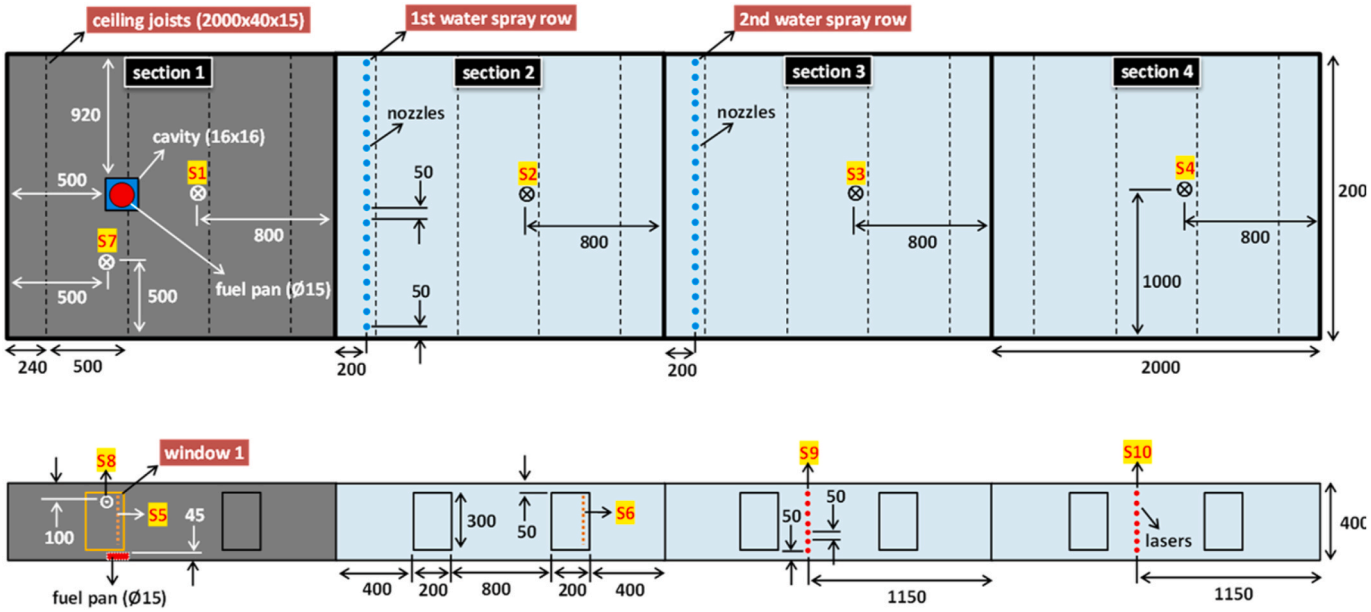

Fig. 6. Deck-end fire scenario 1 with sensors S1 to S10 defined in Fig. 1 (dimensions are in millimeters): the fire is in section 1 and the water mist curtains are 2 m apart.

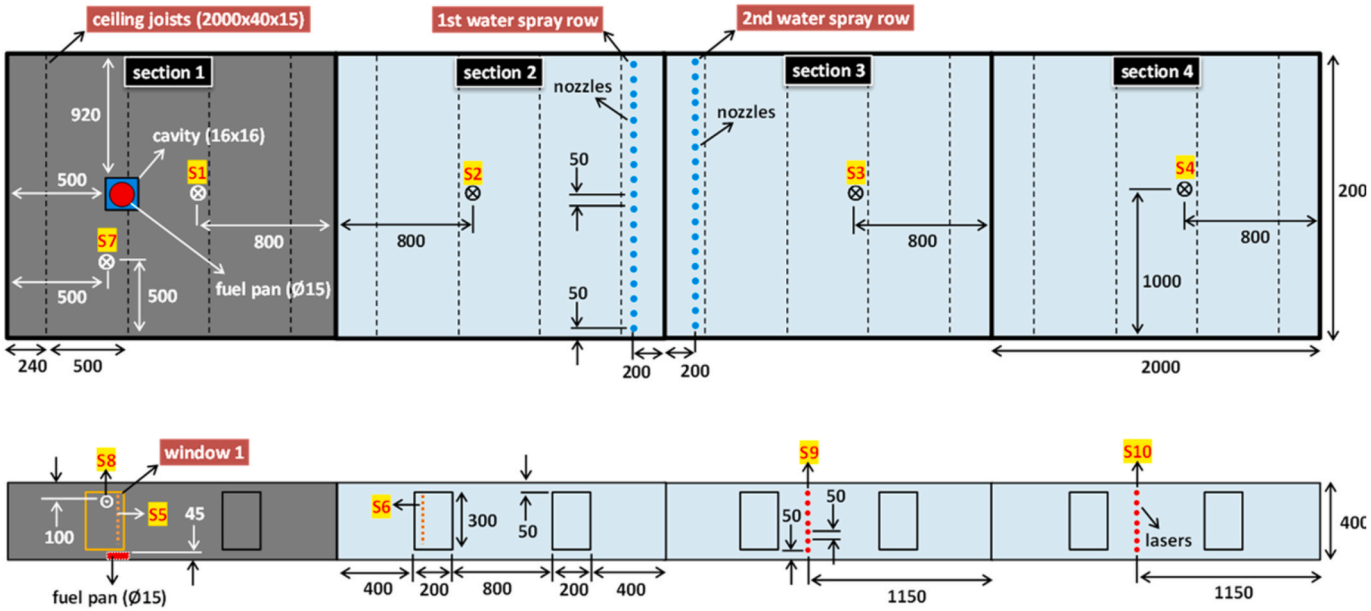

Fig. 7. Deck-end fire scenario 2 with sensors S1 to S10 defined in Fig. 1 (dimensions are in millimeters): the fire is in section 1 and the water mist curtains are 0.4 m apart.

ticles resulting from incomplete combustion. This is done by investigating the attenuation of the opacimeter laser beams. According to Lambert–Beer law, when the beam of light travels through smoke, the intensity of light is reduced with distance as follows:

$$I(x) = I_0 e^{(-\mu x)} \tag{1}$$

where $I(x)$ is the remaining intensity of light after traveling to distance x through smoke, I_0 is the initial intensity of light at $x = 0$ m, and μ is the attenuation coefficient of smoke. This concept can be used to calculate the volume fraction of soot as shown by Krishnan et al. [14]:

$$f_v = -\lambda \cdot \ln(I_L / I_0) / (L \cdot K_e) \tag{2}$$

where f_v is the soot volume fraction, λ is the wavelength of the laser beam (i.e., 640 nm in this study), I_L is the remaining intensity of light after traveling through smoke for distance L (taken to be equal to the deck's width which is 2 m, assuming that smoke is homogeneous), and $K_e \approx 8.4$ is the dimensionless extinction coefficient which is relatively independent of wavelength and fuel type [14].

An example evolution of soot volume fractions obtained using Eq. (2) is shown in Fig. 11 for a deck-end fire (scenario 'E1' described in the captions of Table 4) with open windows and no cargo, facing a single water mist curtain with a pressure of 8 bars. After the ignition of the fire ($t = 0$ s), the mass fraction of soot begins to increase (see Fig. 11). This increase is progressive. Moreover, the opacimeters close to the ceiling show higher concentrations than those of the opacimeters close to the floor. This is due to the stratification of the smoke. However, when the sprays are activated ($t = 180$ s), the curves converge. This is because the

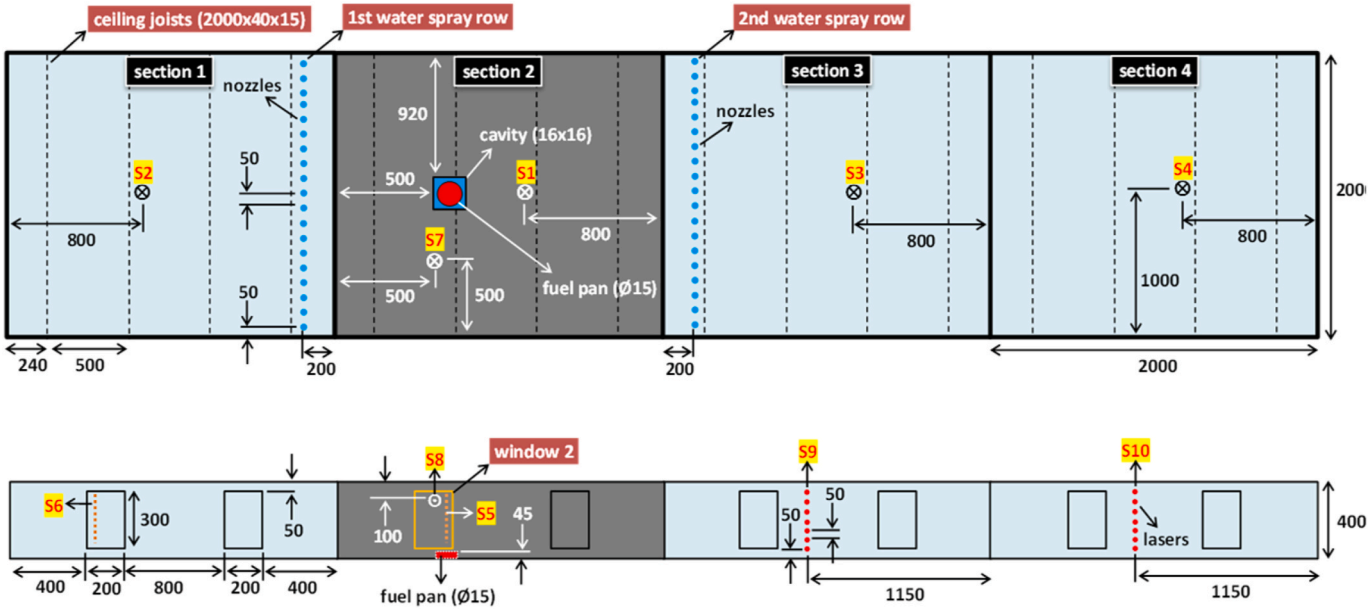

Fig. 8. Deck-middle fire scenario with sensors S1 to S10 defined in Fig. 1 (dimensions are in millimeters): the fire is in section 2 and the water mist curtains are 2.4 m apart.

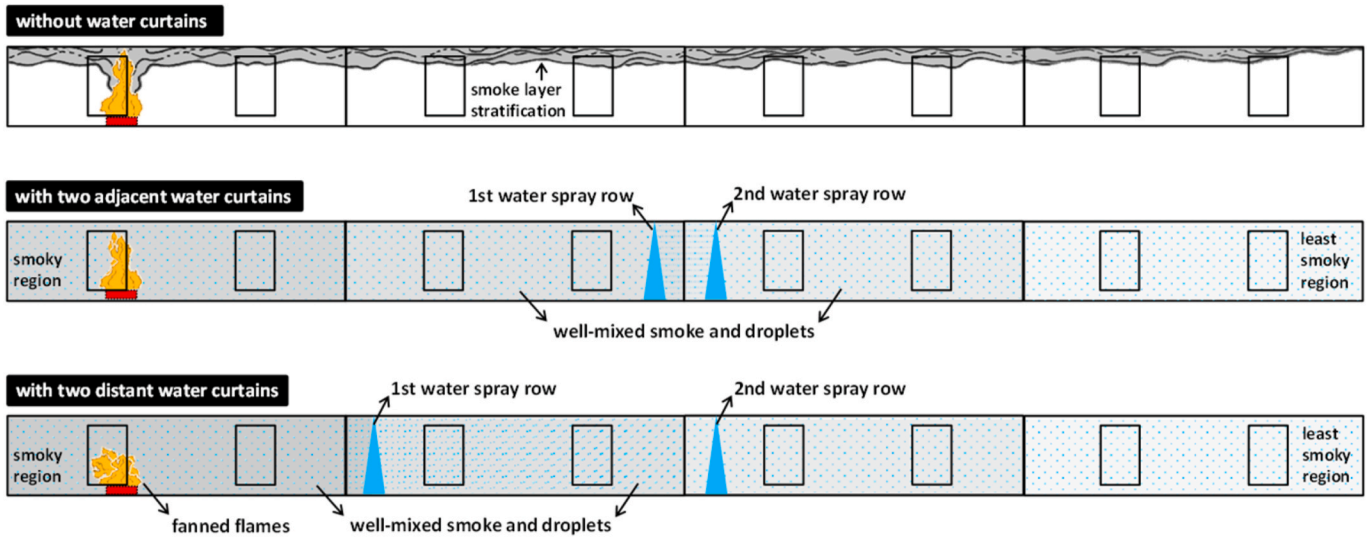

Fig. 9. Smoke dynamics in deck-end fire scenarios with and without water mist curtains.

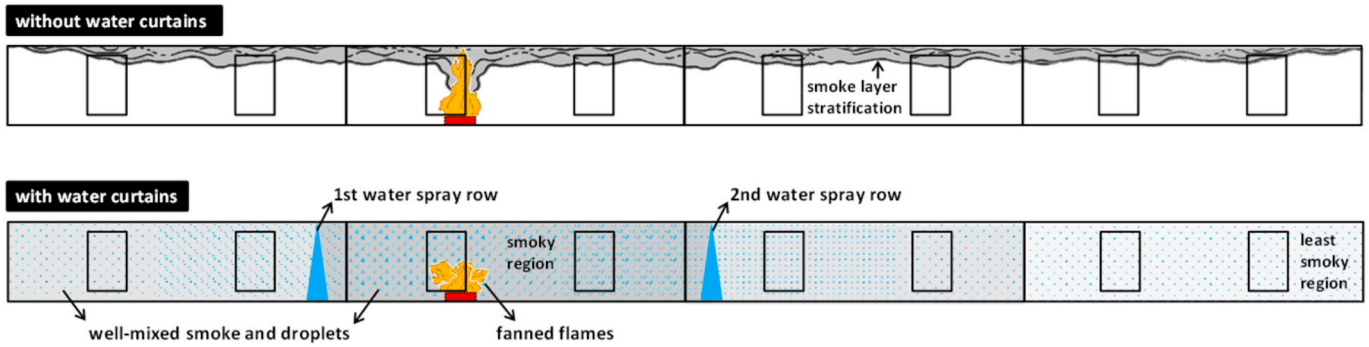

Fig. 10. Smoke dynamics in deck-middle fire scenarios with and without water mist curtains.

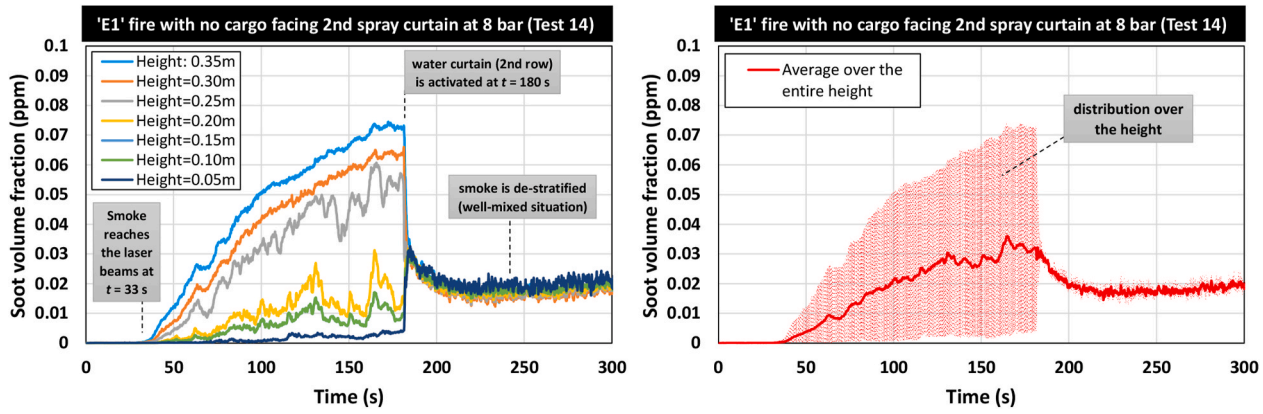

Fig. 11. Evolution of soot volume fractions at different heights in the deck during test 14, obtained using Eq. (2) based on the data of opacimeter beams ('S9' shown in Fig. 6).

soot concentration becomes uniform across the height almost instantly. Accordingly, the soot volume fraction profiles confirm that activating the water mist curtain creates a well-mixed environment as shown in Figs. 9 and 10. Moreover, if the curtain is further away from the fire, the amount of smoke going through the curtain decreases significantly, often reaching a steady soot volume fraction which is half of that in a test without a curtain, e.g., 0.02 ppm in test 14 versus 0.04 ppm in test 11-2, respectively (see Figs. 11 and 12).

If the water mist curtain is located near the fire and there are no cargo items in the deck, the HRR of the fire increases significantly once the water mist curtain is activated (see Fig. 12). In this case, the amount of smoke going through the curtain is initially decreased, while later the increase in the HRR causes the amount of smoke to increase again, surpassing that of the case with no curtain (see the soot volume fraction values in Fig. 12 after $t = 250$ s). Note that the increase in the HRR is due to the turbulent mixing and rapid pulling of air into the deck through the windows caused by the water mist curtain's high-velocity spray. The turbulence disturbs the natural plume of the fire by fanning the flames (as illustrated in Figs. 9 and 10) and allows for better mixing of air and fuel for combustion as well as heat feedback to the fuel, thereby increasing the HRR. This is known as a 'kinetic effect' [12], and is significant when the water spray operates at a high pressure (above 5 bar in this study). This effect is not observed when the deck is fully loaded with cargo (see HRR profiles in Fig. 26), because the cargo items surround the fire and shield it from the momentum of the spray, reducing the aforementioned turbulent mixing.

The temperature measurements across the height of the deck suggest that the activation of the water mist curtain not only creates a well-mixed environment but also causes extensive cooling within the deck, leading to more or less uniform temperatures in every given section, except in the fire section (see Fig. 13).

The height of a stratified smoke layer can be determined from the measurements of gas temperatures along the height of the deck according to several different methods discussed in the literature [15–19]. Based on the findings of the comparative study performed by Haouari Harrak et al. [19], we determine the smoke layer height using the method of Quintiere et al. [16]:

$$\int_0^H \frac{1}{T_{gas}(z)}dz = \frac{H - z_{int}}{T_{up}} + \frac{z_{int}}{T_{low}} \tag{3}$$

$$\int_0^H T_{gas}(z)dz = (H - z_{int}) \cdot T_{up} + z_{int} \cdot T_{low} \tag{4}$$

where z_{int} is the smoke interface height to be determined by combining formulas (3) and (4), H is the total height of the deck (i.e., 0.4 m), $T_{gas}(z)$ is the gas temperature measured at height z in the deck, and ambient gases, T_{up} is a uniform temperature considered for the upper layer containing the smoke, and T_{low} is a uniform temperature considered for the lower layer containing ambient gases. As shown in Ref. [17], Eq. (3) follows from the conservation of mass for the gas flowrates above and below the interface height, while Eq. (4) follows from the conservation of energy using the average gas temperatures along the height to estimate the uniform temperature suitable for the upper layer, i.e., T_{up}. In our study, the results of smoke layer heights agree best with visual observations when T_{low} is taken to be 10% higher than the average of the thermocouple readings along the height at the beginning of each experiment.

Fig. 14 shows the evolution profiles of smoke layer height inside the deck determined based on Eqs. (3) and (4) for test 15. As Fig. 14

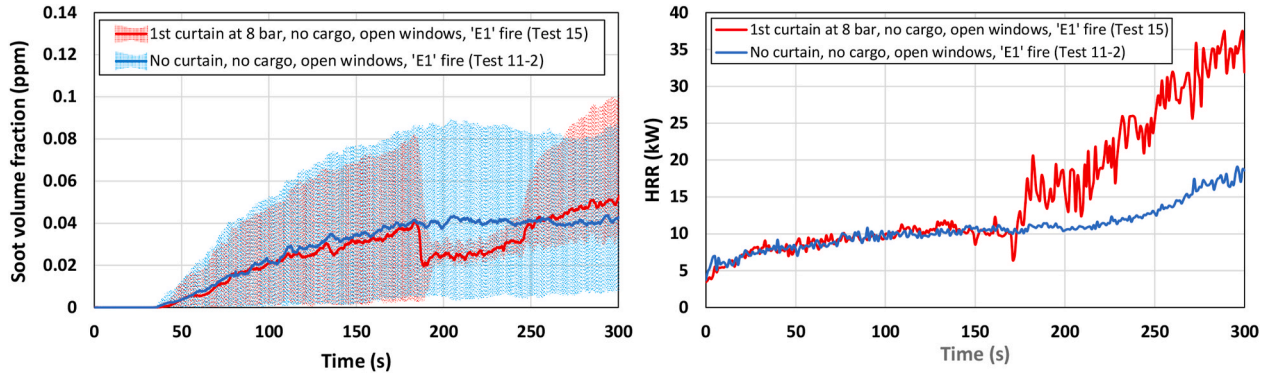

Fig. 12. Evolution of soot volume fraction behind the curtain (left) and the evolution of fire HRR (right) for tests 11-2 and 15.

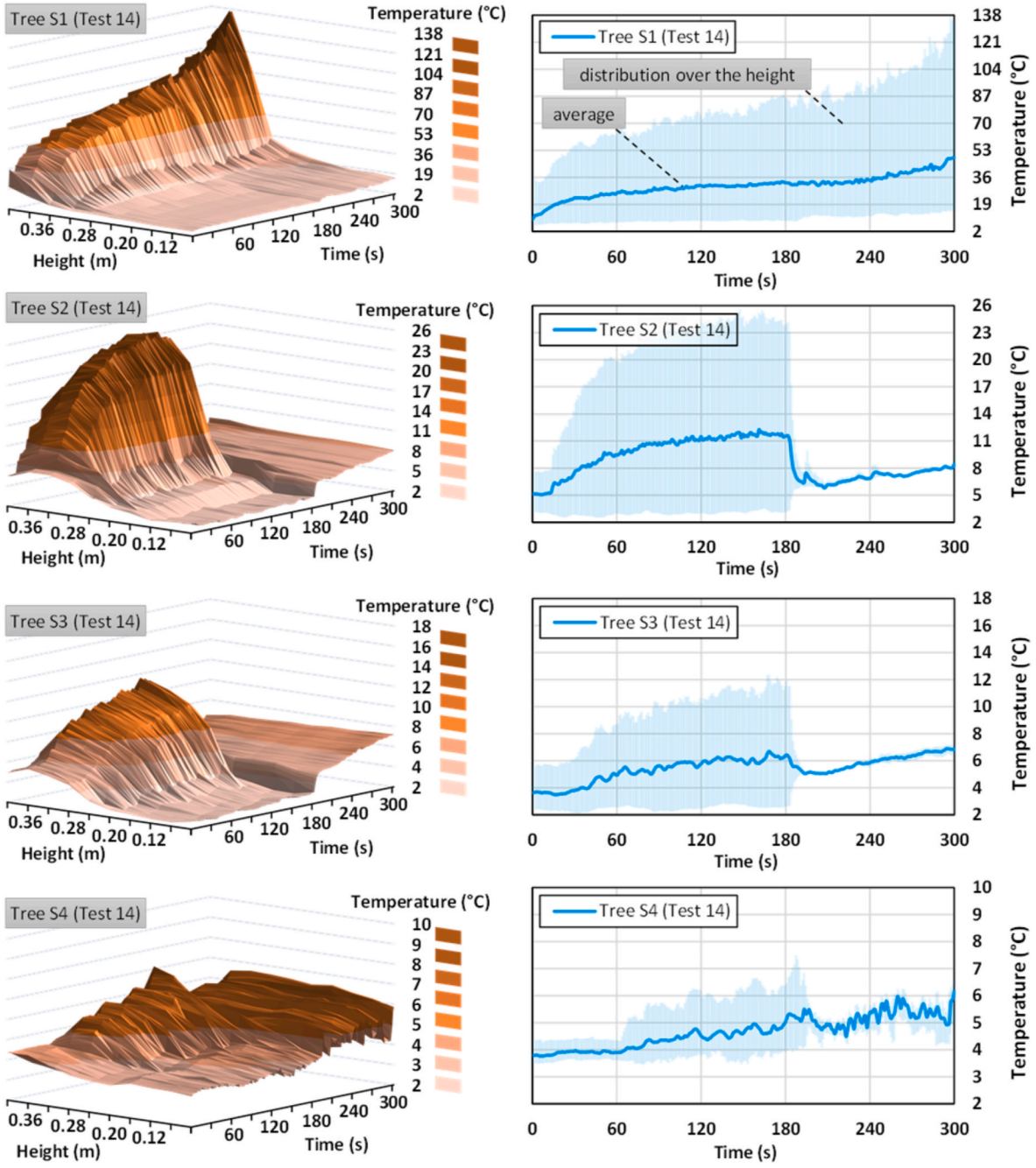

Fig. 13. Temperatures inside the deck in test 14 measured using thermocouple trees S1 to S4 in sections 1 to 4 (as shown in Fig. 6).

indicates, the activation of the water mist curtain causes the smoke layer height to drop to the floor level in every section very rapidly. This is in line with the observation that the smoke is dispersed to the entire deck once the water mist curtain is activated (as illustrated in Figs. 9 and 10).

The concentrations of carbon monoxide measured near the fire are well below 0.3% by volume in all the experiments (see Fig. 15), suggesting that the level of dilution is significant, and that the level of incomplete combustion is not substantial. Therefore, the fire is considered well-ventilated. This is in line with the observation that a pool fire experiment conducted in the open air under a calorimetry hood produced a HRR profile similar to that produced by a pool fire experiment conducted inside the deck setup (see Fig. 16). The HRR in the former case is estimated based on oxygen depletion calorimetry as described in ISO 5660-1 [20], while that in the latter case is estimated by the multiplication of the measured Mass Loss Rate (MLR) in kg/s by the fuel's effective heat of combustion ($\Delta H_C \approx 42{,}640$ kJ/kg for diesel [21]). Correspondingly, the HRRs in the next section are estimated using method 1, assuming $\Delta H_C \approx 42{,}640$ kJ/kg for diesel [21] and $\approx 44{,}566$ kJ/kg for heptane [10].

4. Effects from target study parameters

In this section we investigate how the study parameters listed in Table 3 affect the fire behavior explained in section 3 and how containment efficiency changes based on the different configurations available for each parameter (i.e., options 1 to 3 in Table 3).

4.1. Fire location

The worst-case scenario for fire development in this study is when

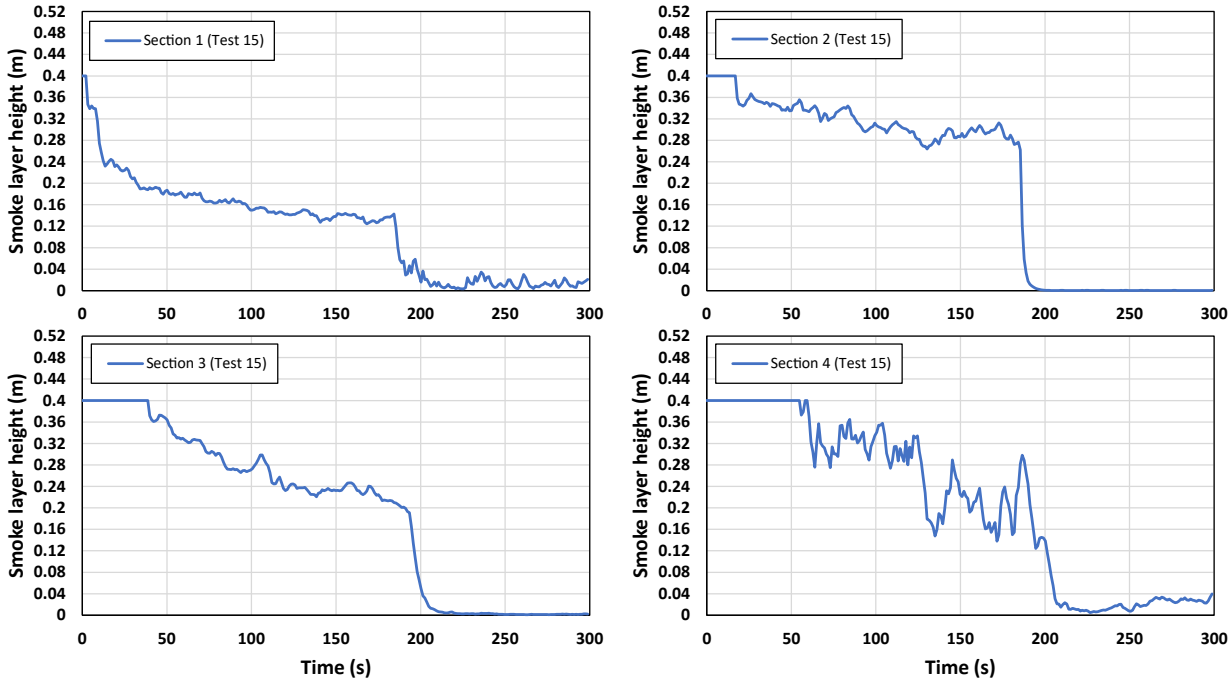

Fig. 14. Smoke layer height inside the deck in sections 1 to 4 in test 15 determined using Eqs. (3) and (4) based on the data of thermocouple trees S1 to S4 shown in Fig. 6.

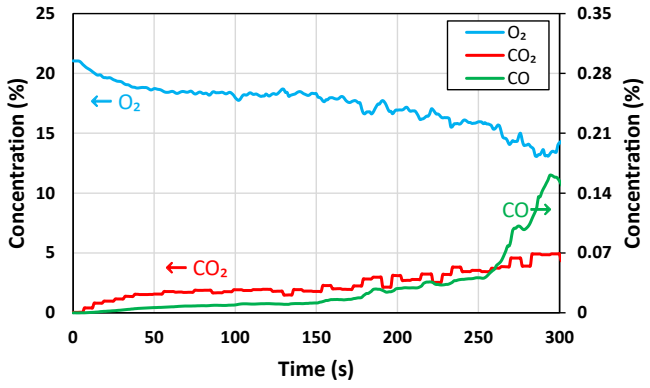

Fig. 15. Concentration of O_2, CO_2 and CO in vicinity of the fire based on the measurements of the gas analyzer S7 shown in Fig. 6.

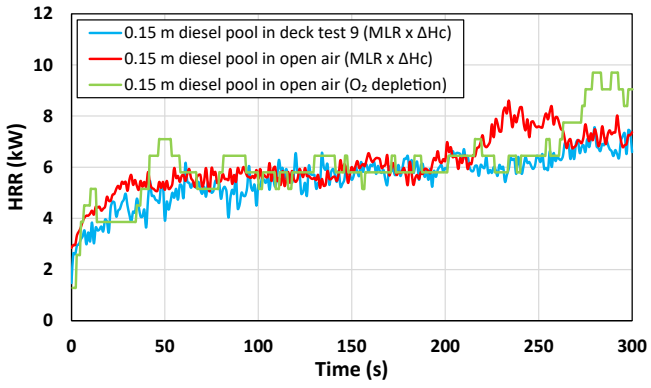

Fig. 16. HRR of a 0.15 m diesel pool fire inside the deck setup versus the HRR of the same pool in the open air under a calorimetry hood.

the fire is located near a closed end of the deck, i.e., scenario 'E1' described in the captions of Table 4. This is when the fire is in the first section of the deck. Here the heat is trapped and provides feedback to the fire, thereby accelerating its development. As this fire location is farthest away from the open end of the deck, it is also less accessible for firefighting intervention and thus challenging to control once it is fully developed.

To demonstrate the fact that fire scenario 'E1' is a worst-case scenario, the amount of smoke produced by this fire is examined by comparing it to that produced by fire scenario 'M1', i.e., when the fire is placed in the second section of the deck in the middle of the setup.

Fig. 17 shows the soot volume fractions across the height of the deck for fire scenarios 'E1' and 'M1' when the evolution of fire HRR is identical for the two scenarios. It is evident in this figure that the soot volume fractions for the case of scenario 'E1' is nearly double that of scenario 'M1'. In other words, the concentration of smoke going through the deck is remarkably higher when the fire is at the end of the deck. This is primarily because in the case of a fire at the end of the deck, all the smoke travels in one direction through the deck, whereas in the case of a fire in the middle of the deck, the smoke is free to move toward either end of the deck, thereby reducing its density in each given direction. Accordingly, fire scenario 'E1' is intrinsically more difficult to contain as it produces a higher unidirectional flowrate of smoke, making it the worst-case scenario in our study. Note that the 'E1' fire shows a later rise in the soot levels compared to the 'M1' fire in Fig. 17 because the fire is located further away from the opacimeter lasers in the 'E1' fire case.

Fig. 18 shows the soot volume fraction and HRR results of a deck-end fire contained using a water mist curtain at a low pressure in comparison to a deck-middle fire contained using two such curtains on both sides (i.e., with a 'straddle' curtain configuration as defined in the captions of Table 4). As the figure indicates, the ultimate steady-state values of soot volume fraction in the deck-end fire scenario are twice as high as those of the deck-middle scenario, indicating that the residual smoke flow through the deck is still clearly higher in the case of the deck-end fire, even though the HRR in this test has been 20% lower than that of the deck-middle fire (see Fig. 18). Moreover, the deck-end fire scenario shows a much bigger drop in the soot volume fraction values shortly after the activation of the curtain. Moreover, it is noteworthy that the

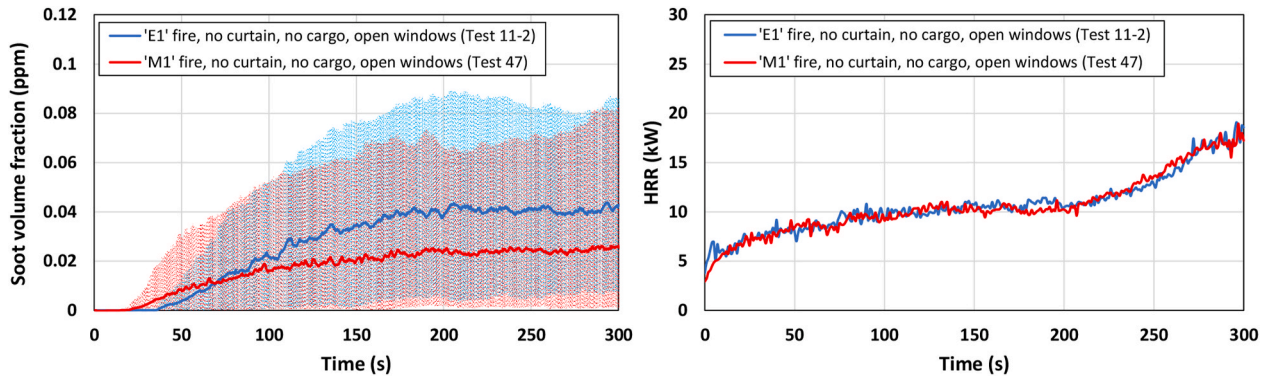

Fig. 17. Evolution of soot volume fraction at the location of 'S9' shown in Fig. 6 (left) and the evolution of fire HRR (right) in the case of a fire near a closed end of the deck (test 11-2) and the case of a fire in the middle of the deck (test 47).

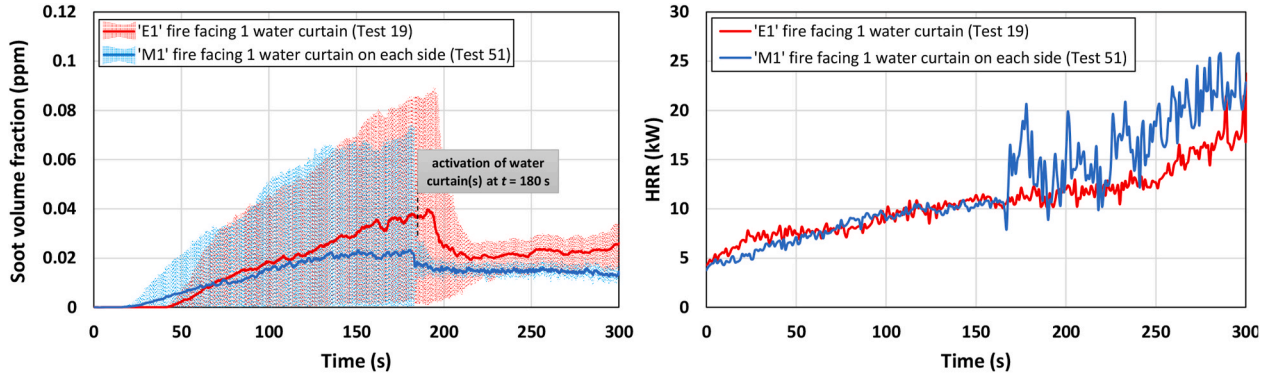

Fig. 18. Evolution of soot volume fraction behind the curtain (left) and the evolution of fire HRR (right) for tests 19 and 51.

'M1' fire shows an earlier rise in the soot levels compared to the 'E1' fire in Fig. 18 because the fire is located closer to the opacimeter lasers in the 'M1' fire case.

The increase in the HRR observed in the case of a deck-middle fire is due to the turbulent mixing and rapid pulling of air into the deck through the windows caused by the water mist curtains straddling the fire. These turbulences disturb the natural plume of the fire and allow for better mixing of air and fuel for combustion, thereby facilitating fuel vaporization which increases the HRR. This effect is much more pronounced when the water pressure of the curtain is increased (see explanations for Fig. 12).

4.2. Deck ends

In principle, the cargo deck could be open at one or both ends, and this has an effect on fire development and containment. Correspondingly, several experiments have been considered to quantify the influence of having a deck configuration with one, two, or no closed ends. In particular, let us consider the deck-end fires 'E1', 'E2' and 'E0' as defined in the captions of Table 4, following the observation that this fire location is strategic from the viewpoint of fire prevention (as discussed in section 4.1).

As Fig. 19 indicates, when there are no curtains activated, a deck with 1 closed end has a slightly higher HRR than that of a deck with open ends (i.e., 'E1' versus 'E0', respectively). This suggests that closing the deck from one side is slightly worse than having it open. Similarly, when

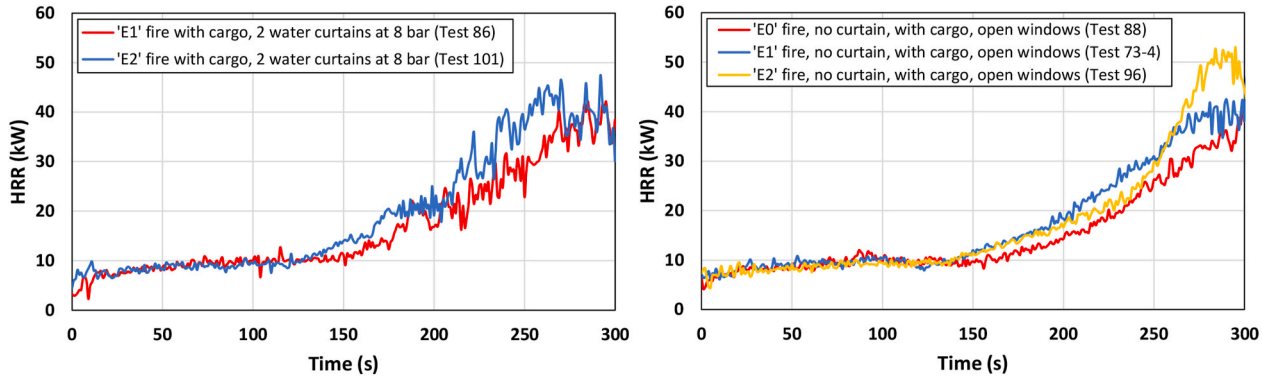

Fig. 19. HRR profiles of deck-end fire scenarios with one end of the deck closed ('E1'), both ends of the deck closed ('E2'), and no ends closed ('E0'). There is no data for 'E0' with curtains.

both ends are closed, i.e., 'E2' configuration, the accumulation of heat causes the HRR to increase significantly at the end of the experiment (t ≈ 270 s). When two water mist curtains at 8 bar are used for containment, a deck with two closed ends (i.e., 'E2') shows a 20% reduction in the HRR with respect to when there is no curtain (see Fig. 19). For a deck with one end closed, using a water mist curtain does not significantly affect the HRR.

The concentrations of O_2 and CO are shown in Fig. 20 for 'E0', 'E1' and 'E2' fire configurations. As Fig. 20 indicates, the 'E2' fire which has the highest HRR leads to the lowest levels of O_2 (as low as 9.8%), while the 'E1' fire which has a lower HRR leads to the highest levels of CO (as high as 2612 ppm). The 'E0' fire has lots of ventilation and the heat in this configuration is not accumulated as much as 'E1' and 'E2' configurations, so it leads to the lowest reduction of O_2 and minimum production of CO (see Fig. 20).

4.3. Fire size and fuel type

It is generally expected that fires produce more smoke at higher HRRs with the same fuel [10]. This is because smoke production is a direct function of the fuel Mass Loss Rate (MLR), which itself defines the HRR. In the case of particulate smoke, this is often approximated through a constant soot yield, i.e., amount of soot per amount of fuel. This constant, however, is fuel dependent. Accordingly, two fires with different fuels but identical HRRs may produce very different quantities of soot, yielding different opacity levels. For example, Fig. 21 indicates that a small diesel fire (0.13 m pool) produces a slightly thicker smoke than does a bigger heptane fire (0.15 m pool), showing higher levels of soot volume fraction especially near the ceiling.

Note that the data of soot volume fraction alone does not generally allow a direct comparison of two different fuels in terms of their total smoke production (i.e., particulate or otherwise). This is because soot is only a representative of the particulate form of smoke, and different fuels may produce different amounts of soot per liter of smoke. That being said, as long as a single fuel is being examined, the data of soot volume fraction can quantify the 'relative difference' of two experiments. Similarly, the data of soot volume fraction can quantify the 'temporal variation' in the amount of smoke during a single experiment. For instance, considering the data of diesel fires presented in Fig. 21, one can conclude that the smoke flow through the deck during the final 100 s is slightly higher for the test performed with a bigger pool, because of its higher HRR after the activation of the water mist curtains.

It is also evident from Fig. 21 that the heptane pool fires grow significantly bigger as the water mist curtains are activated, showing a 200% increase in the HRR. This effect is much more pronounced for heptane than diesel (see Fig. 21), simply because of the higher volatility of heptane, making it more sensitive to the turbulence caused by the water mist curtains which induces turbulent mixing and rapid pulling of fresh air into the deck through the windows (see explanations for Fig. 12). Similarly, additional tests conducted with wood cribs showed that the activation of the spray has a marginal effect on the HRR, again mostly because of the lower volatility of the wood fuel.

4.4. Windows

Several experiments have been conducted to quantify the influence of side openings, hereafter referred to as 'windows' (see Fig. 3). This is to evaluate whether it is advisable to invest on accommodating larger and more frequent windows on the sides of a ro-ro ship or investing on making the windows closable. More specifically, the area of the windows has been fixed at either 0% or 15% of the total area of the sides of the deck in the experiments. These choices correspond to 'closed' and 'open' decks based on SOLAS II-2/3 requirements, respectively (refer to section 1 for the motivation).

When the windows are closed, the activation of the high-pressure curtain doubles the HRR in the first 5 s but then the supply of oxygen becomes insufficient momentarily, so the fire exhibits an oscillatory (i.e., cyclical) behavior: the HRR goes down and the supply of oxygen improves, allowing the HRR to increase again, thereby reducing the oxygen levels again, so on and so forth (see the HRR curve in Fig. 22 after t = 180 s). This in turn causes the level of smoke production to stabilize, such that there is less smoke going through the deck compared to when no curtain is used (see the soot volume fraction values in Fig. 22 after t = 275 s). This indicates that the water mist curtain solution is most effective with closed windows, i.e., in a 'closed deck' configuration, although total flame extinction was never observed in either of the tests.

The experiments conducted with and without open side windows suggest that the fire can achieve a substantially higher peak HRR when the windows are open, sometimes showing a 40% higher peak HRR compared to when the windows are closed (see Fig. 22). This indicates that it is safer to have fewer windows when there are no curtains. The same situation is observed when water mist curtains are used for containment (see Fig. 23).

4.5. Curtain rows and distance

Given a certain total amount of water flowrate, the choice of two curtains provides more effective smoke containment than the choice of a single curtain (see Fig. 24). Accordingly, two curtains operating at 0.2 L/min/nozzle reduce the level of smoke going through the deck more strongly than a single operating at 0.4 L/min/nozzle. In this case, the two-curtain system has the added benefit of operating at a lower pressure, i.e., 3 bar versus 8 bar, which is valuable not only because it requires a less demanding pressurization system but also because it induces less significant turbulent mixing.

The distance between the curtains does not seem to have a strong impact on the smoke containment capability of the curtains. More

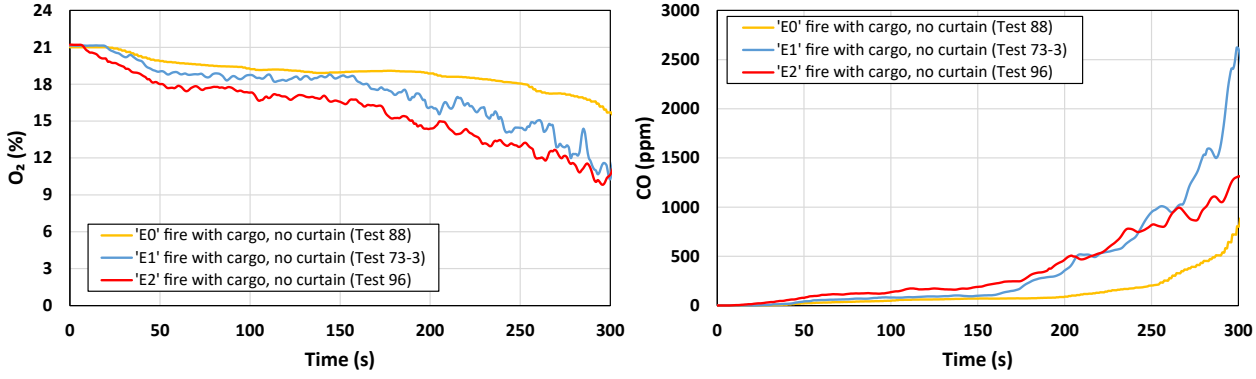

Fig. 20. Variation of the concentrations of CO and O_2 as a function of time for deck-end fire scenarios 'E1', 'E2', and 'E0' described in Table 4.

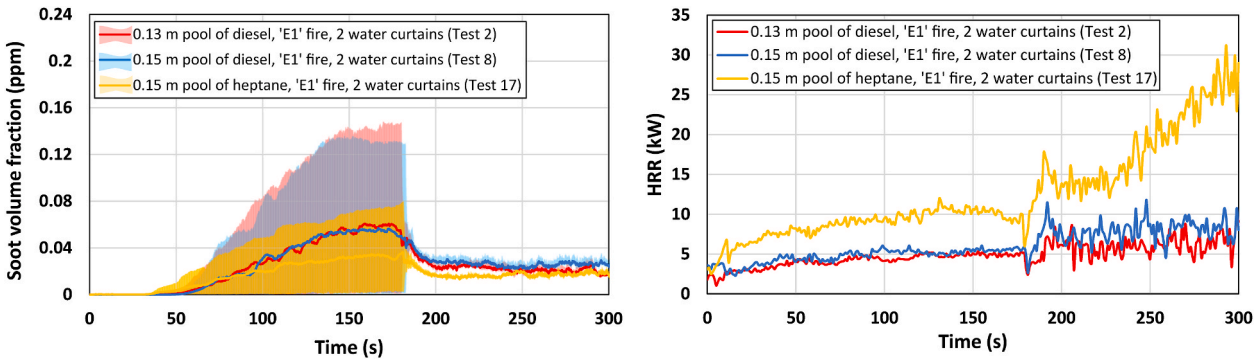

Fig. 21. Evolution of soot volume fraction behind the curtain (left) and the evolution of fire HRR (right) for diesel and heptane pool fires in tests 2, 8 and 17.

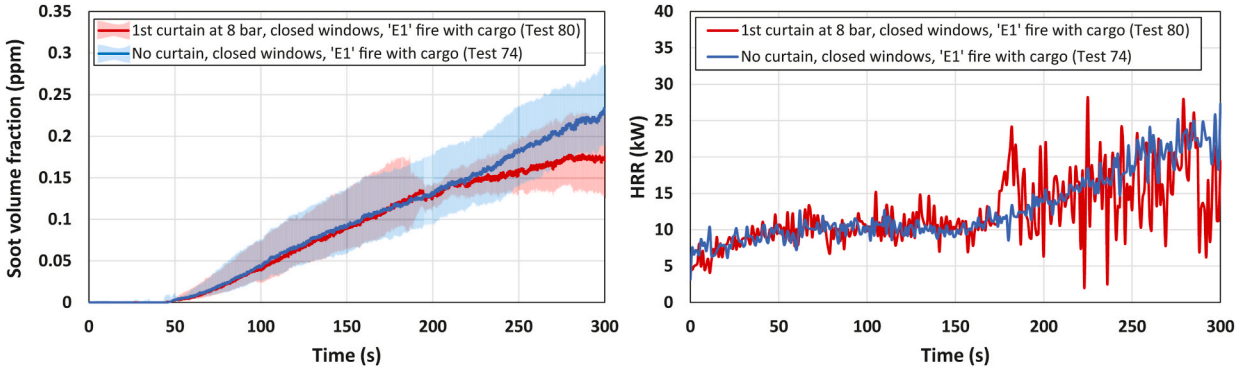

Fig. 22. Evolution of soot volume fraction behind the curtain (left) and the evolution of fire HRR (right) with closed windows with and without curtains in tests 80 and 74, respectively.

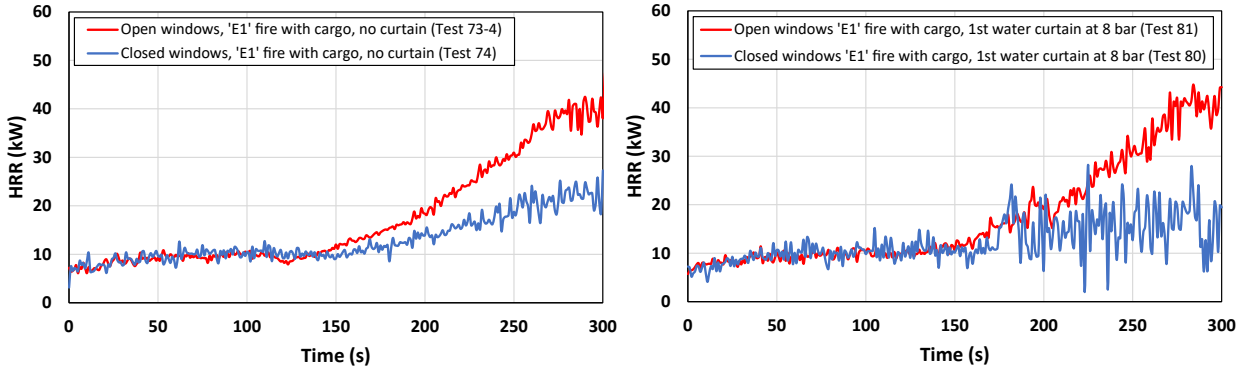

Fig. 23. Fire HRR profiles of deck-end fire scenarios with and without open side windows when there are no curtains (left) and when the first water mist curtain is used (right).

specifically, two curtains separated by a distance of either 0.4 m or 2 m show nearly identical levels of smoke passing though the curtains, regardless of the water flowrate level (see Fig. 25).

4.6. *Water flowrate*

In order to evaluate the effect of water flow rate in the containment efficiency of water mist curtains, a number of experiments have been conducted with flow rates ranging from 0.2 to 0.4 L/min/nozzle. A selection of related experiments with cargo, open windows and a deck-end fire scenario are compared against each other in Fig. 26.

As Fig. 26 indicates, when the windows are open and the deck is fully loaded with cargo items, using the first water mist curtain with a flow rate higher than 0.3 L/min/nozzle causes no change in the amount of smoke shielding or the magnitude of HRR with respect to the scenario with no curtain. However, in the absence of cargo, a high-flowrate curtain induces a strong increase in the HRR (see also explanations for Fig. 12). Accordingly, the only scenario in which the use of a water mist curtain is beneficial is when a low flowrate is used, as smoke and HRR levels are reduced with respect to the case with no curtain (see profiles of low-flowrate curtain in Fig. 26). This is also the case when the windows are closed, where the water mist curtain operated using the lowest flowrate provides the highest level of smoke containment (see Fig. 27). This is expected to be due to the lower pressure of such a curtain that induces less mixing and smoke production.

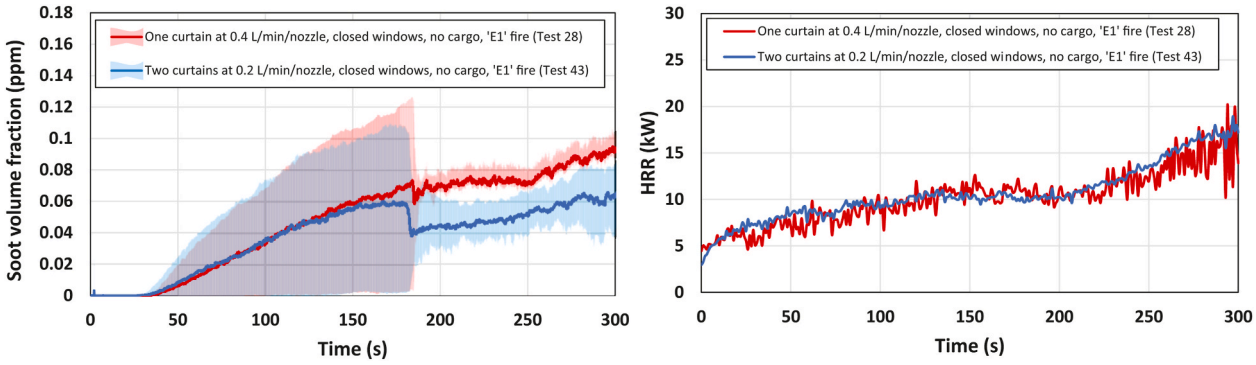

Fig. 24. Evolution of soot volume fraction at location 'S9' shown in Fig. 6 (left) and the evolution of fire HRR (right) in tests with one or two water mist curtains.

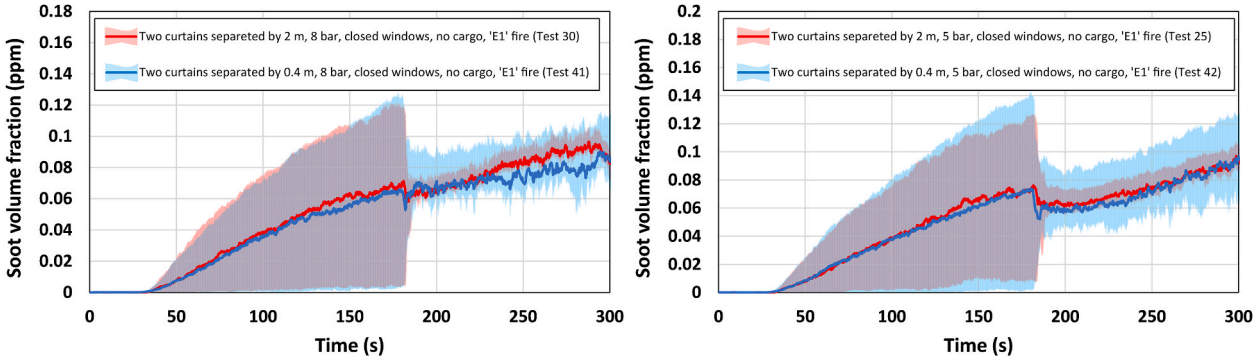

Fig. 25. Evolution of soot volume fraction at location 'S9' shown in Fig. 6 for tests with two water mist curtains separated by 0.4 m and 2 m at water pressures of 8 bar (left) and 5 bar (right).

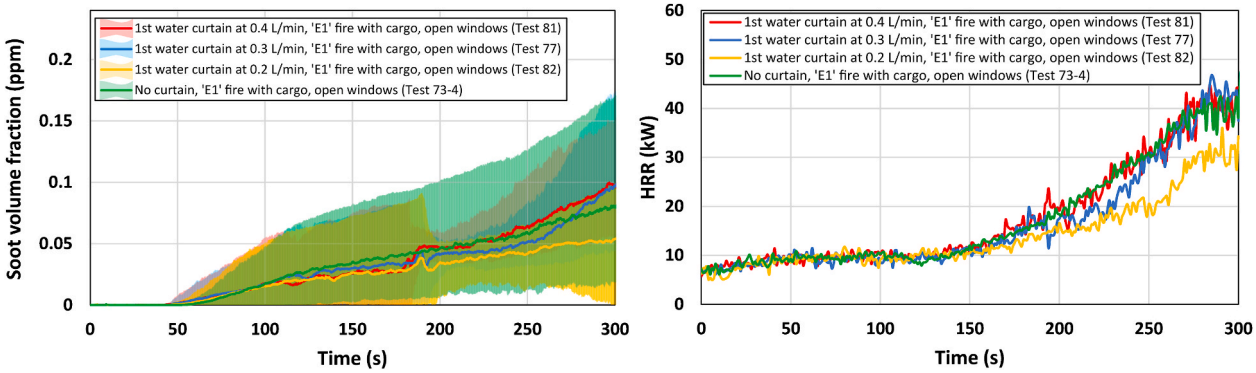

Fig. 26. Evolution of soot volume fraction at location 'S9' shown in Fig. 6 (left) and the evolution of fire HRR (right) for an 'E1' fire contained using either 1 or 2 water mist curtains at flow rates of 0.2, 0.3 and 0.4 L/min/nozzle with open windows.

4.7. Cargo

Several experiments have been conducted with a deck full of cargo blocks, arranged as shown in Fig. 28. This was to quantify how the presence of cargo items can affect the fire and its containment through changes in the flow field, i.e., the cargo items are not allowed to burn in the experiments. To ensure this, concrete blocks are used near the fire source, while expanded polystyrene blocks are used further away, representing trailers and vehicles.

In the presence of cargo in the deck, the kinetic effect of a high-pressure curtain (explained for Fig. 11) is much less pronounced as the fire is shielded behind the cargo items. Accordingly, the HRR is comparable to when there is no curtain, but smoke production is slightly higher with the curtain (see Fig. 29). Correspondingly, when a high-pressure curtain is used near the fire in the presence of cargo, the amount of smoke going through the deck eventually increases beyond that observed with no curtain (see the soot volume fraction values in Fig. 29 after t = 250 s). With no cargo in the deck, a high-flowrate curtain induces a strong increase in the HRR (see Fig. 11).

The experiments conducted with no curtains suggest that the presence of cargo itself has an intensifying effect on the fire growth, resulting in both a higher peak HRR and a higher amount of smoke going through the deck (see Fig. 30). This is because the heat of the fire is confined by the nearby cargo blocks, thereby reducing heat losses and increasing thermal feedback to the fire, which in turn increases the burning rate of the fuel and thus the rate of smoke production. Consequently, the presence of cargo makes fire containment all the more challenging for the curtains.

The intensifying effect of cargo on the fire growth is reduced when a curtain is used for containment (compare Figs. 30 and 31).

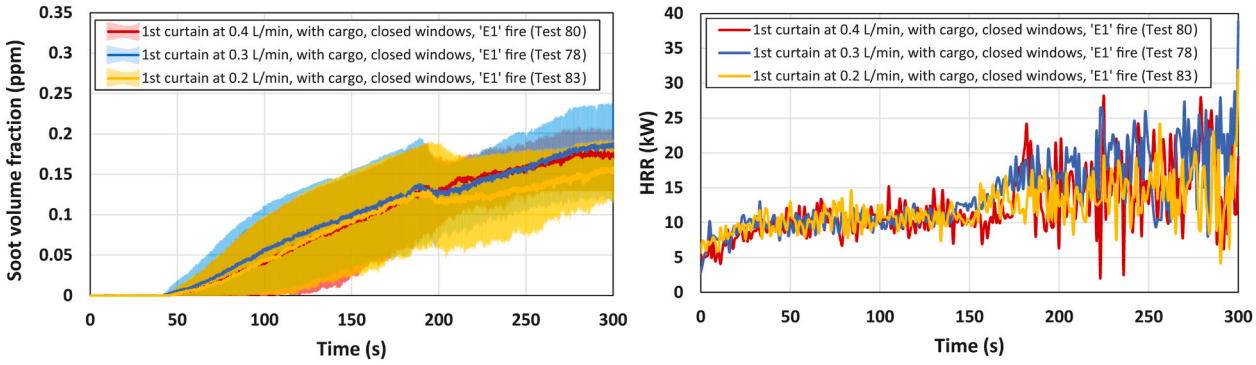

Fig. 27. Evolution of soot volume fraction at location 'S9' shown in Fig. 6 (left) and the evolution of fire HRR (right) for an 'E1' fire contained using either 1 or 2 water mist curtains at flow rates of 0.2, 0.3 and 0.4 L/min/nozzle with closed windows.

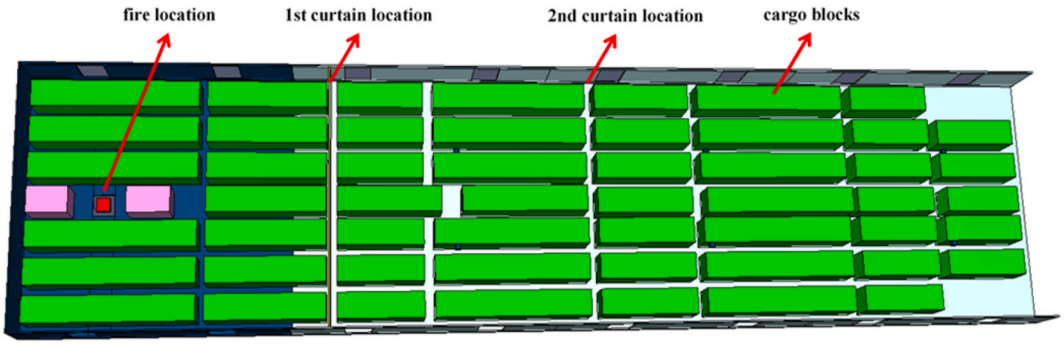

Fig. 28. Arrangement of cargo items in the fully loaded model deck.

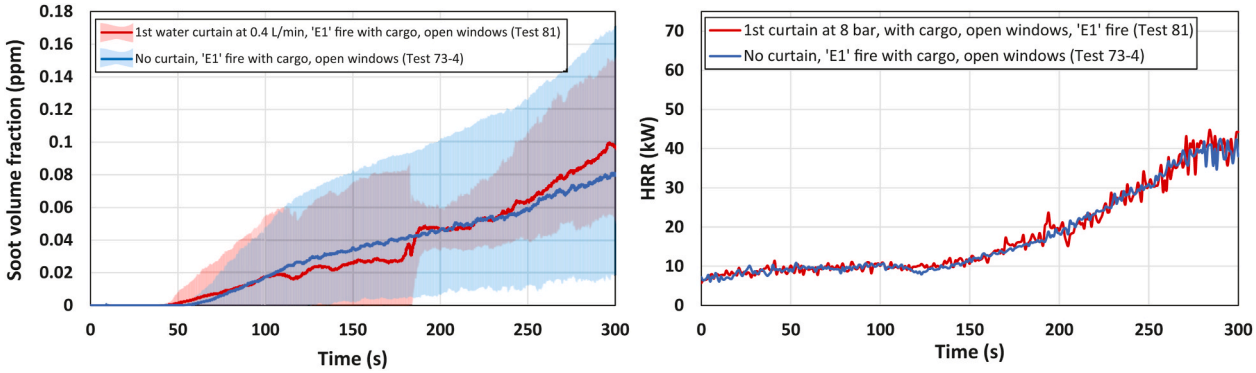

Fig. 29. Evolution of soot volume fraction behind the curtain (left) and the evolution of fire HRR (right) for tests with cargo and open windows, with and without a water mist curtain.

Correspondingly, the use of a water mist curtain controls the peak amount of smoke going through the deck, maintaining a stable flow of smoke for a period longer than 300 s. This suggests that using a water mist curtain is more favorable when the deck is full of cargo.

5. Conclusions

The conducted experiments suggest that a fire near a closed end of the deck is a worse-case scenario in terms of smoke production and the peak Heat Release Rate (HRR), which must be considered in the definitions of hazardous cargo areas on board. Considering the 'open deck' and 'closed deck' configurations specified by the international convention for the Safety of Life at Sea (SOLAS), a closed deck with fewer or no 'side openings' (herein called 'windows') is found to be safer in terms of allowing lower HRRs.

In most of the experiments, water mist curtains reduced the net longitudinal flow of smoke along the deck, although the smoke is dispersed in all directions. The probability of flame spread to sections behind a water mist curtain is reduced because of the strong cooling effect offered by the curtain. This is owing to the wide spray pattern of the nozzles, causing the thermal protection of a water mist curtain to extend a few meters beyond the exact location of the curtain. Furthermore, water mist curtains redirect a major part of the smoke to open windows near the fire in the 'open deck' configuration.

When there is no cargo in the deck, if a high-pressure water mist curtain is activated to isolate a liquid pool fire, the HRR may increase if the pool is too close to the curtain, because the vaporization of the liquid fuel is sensitive to the turbulence in the flow field caused by a high-pressure water spray. When the deck is full of cargo, this increase in the HRR is not observed, although the smoke production is still higher

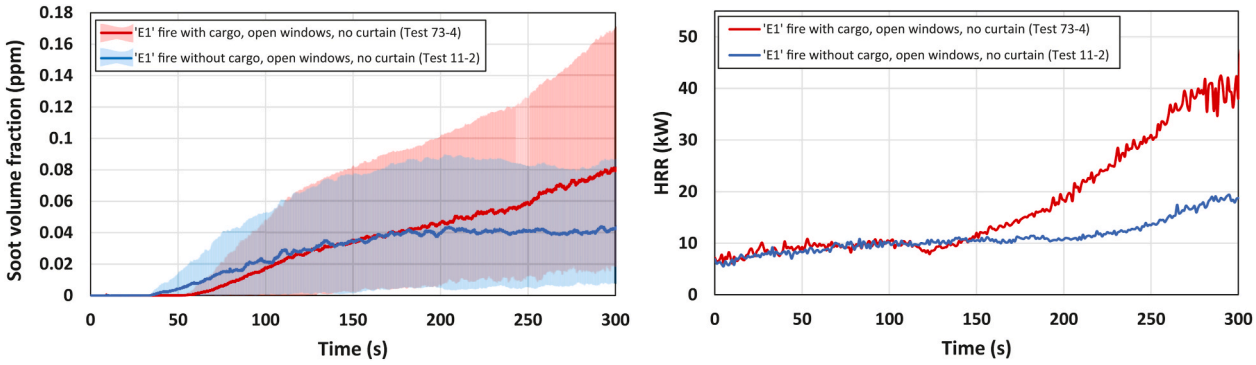

Fig. 30. Evolution of soot volume fraction behind the curtain (left) and the evolution of fire HRR (right) for tests with and without cargo with open windows and no water mist curtain.

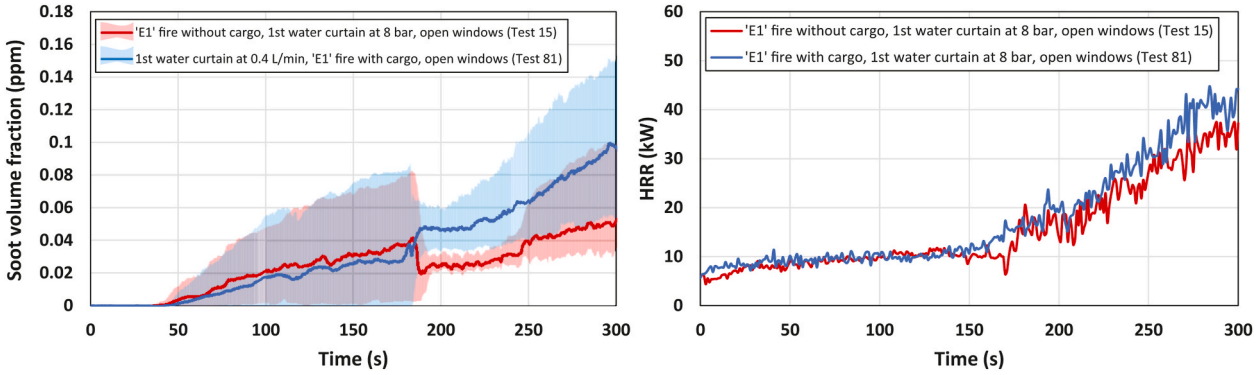

Fig. 31. Evolution of soot volume fraction behind the curtain (left) and the evolution of fire HRR (right) for tests with and without cargo with open windows and one water mist curtain.

when a curtain is used. Moreover, this effect was not observed in experiments conducted with wood as the fuel source, so it is expected that solid fuels will not experience a HRR increase close to a high-pressure water mist curtain.

Distributing the water to several curtains instead of a single curtain with a high pressure appears to be more effective for smoke containment. For the curtains to operate optimally, the area under the water mist curtains is best to be free of cargo. This is because when cargo items are placed below a water mist curtain, lots of droplets land on the cargo items prematurely and cannot float away freely to provide distant radiative shielding and cooling effects. Moreover, in order to minimize the growth of HRR when the water mist curtains activate, windows to the exterior should be in a closed position.

Author statement

Davood Zeinali: Conceptualization, Methodology, Software, Validation, Formal analysis, Investigation, Data Curation, Writing - Original Draft, Writing - Review & Editing, Visualization, Project administration. **Rabah Mehaddi:** Conceptualization, Methodology, Formal analysis, Investigation, Writing - Review & Editing, Project administration. **Florian Ingold:** Methodology, Investigation, Writing - Review & Editing. **Gilles Parent:** Conceptualization, Methodology, Formal analysis, Investigation, Writing - Review & Editing, Project administration. **Zoubir Acem:** Conceptualization, Methodology, Formal analysis, Investigation, Writing - Review & Editing, Project administration. **Anthony Collin:** Methodology, Investigation, Writing - Review & Editing. **Jose Luis Torero:** Methodology, Validation, Formal analysis, Investigation, Writing - Review & Editing. **Pascal Boulet:** Conceptualization, Resources, Writing- Reviewing and Editing, Supervision, Project administration, Funding acquisition.

Declaration of competing interest

The authors declare the following financial interests/personal relationships which may be considered as potential competing interests: Davood Zeinali reports financial support was provided by Horizon 2020.

Funded by the European Union

Data availability

Data will be made available on request.

Acknowledgments

This work was funded by European Union's Horizon 2020 research and innovation program through grant agreement no. 814975 as part of the international research project of LASH FIRE. The authors gratefully acknowledge the insights from Martin Carlsson (Stena Line Naval Architect).

References

[1] NFPA 750, Standard on Water Mist Fire Protection Systems, National Fire Protection Association, Quincy, Massachusetts, US, 2023.
[2] E. Blanchard, P. Boulet, P. Fromy, S. Desanghere, P. Carlotti, J.P. Vantelon, J. P. Garo, Experimental and numerical study of the interaction between water mist and fire in an intermediate test tunnel, Fire Technol. 50 (3) (2014/05/01 2014) 565–587, https://doi.org/10.1007/s10694-013-0323-z.
[3] G. Parent, R. Morlon, Z. Acem, P. Fromy, E. Blanchard, P. Boulet, Radiative shielding effect due to different water sprays used in a real scale application, Int. J.

Therm. Sci. 105 (2016/07/01/2016) 174–181, https://doi.org/10.1016/j.ijthermalsci.2016.02.008.
[4] R. Mehaddi, A. Collin, P. Boulet, Z. Acem, J. Telassamou, S. Becker, F. Demeurie, J.-Y. Morel, Use of a water mist for smoke confinement and radiation shielding in case of fire during tunnel construction, Int. J. Therm. Sci. 148 (2020/02/01/2020), 106156, https://doi.org/10.1016/j.ijthermalsci.2019.106156.
[5] G. Parent, P. Boulet, S. Gauthier, J. Blaise, A. Collin, Experimental investigation of radiation transmission through a water spray, J. Quant. Spectrosc. Radiat. Transf. 97 (1) (2006/01/01/2006) 126–141, https://doi.org/10.1016/j.jqsrt.2004.12.030.
[6] A. Collin, P. Boulet, G. Parent, D. Lacroix, Numerical simulation of a water spray—radiation attenuation related to spray dynamics, Int. J. Therm. Sci. 46 (9) (2007/09/01/2007) 856–868, https://doi.org/10.1016/j.ijthermalsci.2006.11.005.
[7] D. Zeinali, F. Inglod, Z. Acem, R. Mehaddi, G. Parent, A. Collin, P. Boulet, Experimental study of radiation attenuation using water mist curtains in a reduced-scale deck of a ro-ro ship, in: Presented at the Proceedings of the 1st International Conference on the Stability and Safety of Ships and Ocean Vehicles, 2021. Glasgow, Scotland, UK, June 7-11, 2021.
[8] IMO, International convention for the safety of Life at Sea (SOLAS), Chapter II-2, Part A, Regulation 3, 1974, as Amended in 2022, https://www.imo.org/en/OurWork/Safety/Pages/summaryofsolaschapterii-2-default.aspx.
[9] J.G. Quintiere, Scaling applications in fire research, Fire Saf. J. 15 (1) (1989/01/01/1989) 3–29, https://doi.org/10.1016/0379-7112(89)90045-3.
[10] D. Drysdale, An Introduction to Fire Dynamics, third ed., Wiley Online Books: John Wiley & Sons, Ltd, 2011, pp. 35–82.
[11] H.-Z. Yu, Froude-modeling-based general scaling relationships for fire suppression by water sprays, Fire Saf. J. 47 (2012/01/01/2012) 1–7, https://doi.org/10.1016/j.firesaf.2011.09.006.
[12] J.R. Mawhinney, G.G. Back, Water mist fire suppression systems, in: M.J. Hurley, et al. (Eds.), SFPE Handbook of Fire Protection Engineering, Springer New York, New York, NY, 2016, pp. 1587–1645.
[13] G. Parent, R. Morlon, P. Fromy, E. Blanchard, P. Boulet, Multi-point opacity measurement in a fire environment using a network of optical fibres, Fire Saf. J. 83 (2016/07/01/2016) 7–14, https://doi.org/10.1016/j.firesaf.2016.04.003.
[14] S.S. Krishnan, K.-C. Lin, G.M. Faeth, Optical properties in the visible of overfire soot in large buoyant turbulent diffusion flames, J. Heat Tran. 122 (3) (2000) 517–524, https://doi.org/10.1115/1.1288025.
[15] L.Y. Cooper, M. Harkleroad, J. Quintiere, W. Rinkinen, An experimental study of upper hot layer stratification in full-scale multiroom fire scenarios, J. Heat Tran. 104 (4) (1982) 741–749, https://doi.org/10.1115/1.3245194.
[16] J.G. Quintiere, K. Steckler, D. Corley, An assessment of fire induced flows in compartments, Fire Sci. Technol. 4 (1) (1984) 1–14, https://doi.org/10.3210/fst.4.1.
[17] M. Janssens, H.C. Tran, Data reduction of room tests for zone model validation, J. Fire Sci. 10 (6) (1992/11/01 1992) 528–555, https://doi.org/10.1177/073490419201000604.
[18] Y. He, A. Fernando, M. Luo, Determination of interface height from measured parameter profile in enclosure fire experiment, Fire Saf. J. 31 (1) (1998/07/01/1998) 19–38, https://doi.org/10.1016/S0379-7112(97)00064-7.
[19] S. Haouari Harrak, R. Mehaddi, P. Boulet, E.M. Koutaiba, G. Giovannelli, S. Becker, Virtual origin correction for a fire plume in a room under displacement ventilation regime, Int. J. Therm. Sci. 136 (2019/02/01/2019) 243–253, https://doi.org/10.1016/j.ijthermalsci.2018.10.023.
[20] ISO 5660-1, "Reaction-to-fire Tests – Heat Release, Smoke Production and Mass Loss Rate – Part 1: Heat Release Rate (Cone Calorimeter Method) and Smoke Production Rate (Dynamic Measurement),", International Standards Organization (ISO), Geneva, Switzerland, 2015.
[21] M. Canakci, M. Hosoz, Energy and exergy analyses of a diesel engine fuelled with various biodiesels, Energy Sources B Energy Econ. Plann. 1 (4) (2006) 379–394, https://doi.org/10.1080/15567240500400796.